

Inorganic carbon and pH dependency of *Trichodesmium*'s photosynthetic rates.

Running title: Photosynthetic rates as a function of pH and HCO_3^- .

TOBIAS G. BOATMAN^{1*}, NIALL M. MANGAN², TRACY LAWSON¹, RICHARD J. GEIDER¹

¹School of Biological Sciences, University of Essex, Wivenhoe Park, Colchester, Essex, CO4 3SQ, UK

²Department of Engineering Sciences and Applied Mathematics, Northwestern University, Evanston, Illinois, 60208, USA

*To whom correspondence should be addressed: Tobias G Boatman

tboatman@chelsea.co.uk (Tel: 02084 819009); niall.mangan@northwestern.edu; tlawson@essex.ac.uk; geider@essex.ac.uk

Highlight

Trichodesmium's photosynthetic rates appear to be a function of CO_2 , although numerical simulations of the carbon concentrating mechanism (CCM) show carboxylation to be mediated as a function of pH and HCO_3^- .

© The Author(s) 2018. Published by Oxford University Press on behalf of the Society for Experimental Biology.

This is an Open Access article distributed under the terms of the Creative Commons Attribution License (<http://creativecommons.org/licenses/by/4.0/>), which permits unrestricted reuse, distribution, and reproduction in any medium, provided the original work is properly cited.

Abstract

We established the relationship between photosynthetic carbon fixation rates and pH, CO₂ and HCO₃⁻ concentrations in the diazotroph *Trichodesmium erythraeum* IMS101. Inorganic ¹⁴C-assimilation was measured in TRIS-buffered ASW medium where the absolute and relative concentrations of CO₂, pH and HCO₃⁻ were manipulated. First, we varied the total dissolved inorganic carbon concentration (TIC) (< 0 to ~ 5 mM) at constant pH, so ratios of CO₂ and HCO₃⁻ remained relatively constant. Second, we varied pH (~ 8.54 to 7.52) at constant TIC, so CO₂ increased whilst HCO₃⁻ declined. We found that ¹⁴C-assimilation could be described by the same function of CO₂ for both approaches but showed different dependencies on HCO₃⁻ when pH was varied at constant TIC than when TIC was varied at constant pH. A numerical model of *Trichodesmium*'s CCM showed carboxylation rates are modulated by HCO₃⁻ and pH. The decrease in Ci assimilation at low CO₂, when TIC was varied, is due to HCO₃⁻ uptake limitation of the carboxylation rate. Conversely, when pH was varied, Ci assimilation declined due to a high-pH mediated increase in HCO₃⁻ and CO₂ leakage rates, potentially coupled to other processes (uncharacterised within the CCM model) that restrict Ci assimilation rates under high-pH conditions.

Keywords: *Trichodesmium*, Cyanobacteria, Ocean acidification, CO₂, Carbon acquisition, Gross photosynthesis, Net photosynthesis, Carbon concentrating mechanism (CCM)

Accepted Manuscript

Introduction

Over the past 150 years atmospheric CO₂ concentrations have increased from pre-industrial levels (i.e. 280 μmol mol⁻¹) to a current value of about 400 μmol mol⁻¹, and are predicted to increase further to 650 μmol mol⁻¹ by mid-century and to 750/1000 μmol mol⁻¹ by the end of this century (Raven *et al.*, 2005). Equilibration of CO₂ between the atmosphere and ocean is leading to increases in dissolved CO₂ and HCO₃⁻ and decreases in pH and CO₃²⁻. This process of ocean acidification will reduce the pH from average preindustrial levels of 8.2 to about 7.9 by the end of the century (Zeebe *et al.*, 1999; Zeebe and Wolf-Gladrow, 2001). To date, there are still many uncertainties as to the magnitude of biological responses of key organisms to these chemical changes.

One group of organisms of particular importance are the diazotrophic cyanobacteria (photosynthetic dinitrogen-fixers), notably because of their significant contribution to marine primary productivity by converting N₂ into NH₄⁺, thus providing "new" nitrogen to the oceans. The filamentous cyanobacterium *Trichodesmium* is a colony forming species which fixes nitrogen in an area corresponding to half the Earth's surface (Davis and McGillicuddy, 2006), and is estimated to account for more than half of the new (combined) nitrogen production in many parts of the oligotrophic tropical and subtropical oceans (Capone *et al.*, 2005).

Cyanobacteria, *Trichodesmium* sp. included, achieve high photosynthetic rates despite i), the slow diffusion of CO₂ in water (10⁴ times slower than in air) ii), a slow chemical equilibrium between HCO₃⁻ and CO₂ within the 7 – 8.5 pH range and iii), a low affinity of Rubisco for CO₂ relative to ambient CO₂ concentrations. Cyanobacteria employ an intracellular carbon concentrating mechanism (CCM) (Badger and Price, 2003; Badger *et al.*, 2006; Kranz *et al.*, 2010), where enhanced primary productivity significantly outweighs the metabolic costs of CCM activity (Price *et al.*, 2008). The CCM benefits cyanobacteria by reducing photorespiration (Kaplan and Reinhold, 1999; Schwarz *et al.*, 1995), aids in the dissipation of excess light energy as well as maintaining an optimal intracellular pH (Badger *et al.*, 1994; Kaplan and Reinhold, 1999). The consensus is that upregulation of CCM activity in response to a low-CO₂ environment involves two components: firstly, an increase in the transport of inorganic carbon (Ci) from the environment into the cell via a suite of Ci transporters which could involve using ATP (BCT1 HCO₃⁻ transporter), NADPH or reduced ferredoxin (CO₂ conversion from passive diffusion) or coupling to an electrochemical Na⁺ gradient (SbtA or

BicA HCO_3^- transport) to provide the energy for Ci uptake (Badger *et al.*, 2002; Badger and Price, 2003); and secondly, an increased ability to reduce CO_2 leakage from around the site of carboxylation, achieved via arrangement of the molecular components of the carboxysome structure and a CO_2 uptake system located on the thylakoid layer, preventing the efflux of leaked CO_2 to the outer cytosolic layer (Price *et al.*, 2008).

Both ^{14}C isotope disequilibrium experiments and simultaneous measurements of CO_2 and O_2 exchanges during sequential light-dark transitions indicate that HCO_3^- contributes > 90% of the Ci assimilation by *T. erythraeum* IMS101 (Eichner *et al.*, 2015; Kranz *et al.*, 2009). This preference for HCO_3^- is consistent with the evidence that *Trichodesmium* lacks a plasma membrane-bound extracellular carbonic anhydrase (eCA) (Badger *et al.*, 2006; Price *et al.*, 2008). Furthermore, the *T. erythraeum* genome indicates the presence of both a plasma membrane HCO_3^- transporter (BicA) and an intracellular system for conversion of CO_2 to HCO_3^- (NDH-I₄) (Price *et al.*, 2008). These two modes of the CCM result in the accumulation of HCO_3^- in the cytosol, which diffuses to the carboxysome. Inorganic carbon uptake by *Trichodesmium* involves the uptake of HCO_3^- by the BicA transporter. This transporter has a K_m of 40-100 μM HCO_3^- , which is well below the typical concentration of HCO_3^- in seawater (~ 2000 μM) (Badger *et al.*, 2006). Following transport into the cell, C-fixation in *Trichodesmium*, like other cyanobacteria spp., occurs within carboxysomes where HCO_3^- is converted to CO_2 via a carbonic anhydrase followed by fixation of CO_2 by ribulose biphosphate carboxylase oxygenase (Rubisco). Carboxysomes provide microenvironments where CO_2 is elevated to compensate for the low affinity of cyanobacterial Rubiscos for CO_2 ($K_m\text{CO}_2 > 150 \text{ mM}$) (Badger and Andrews, 1987). In *Trichodesmium*, CO_2 that leaks from carboxysomes can be converted to HCO_3^- by the plasma membrane bound NDH-I₄ protein, thus reducing the efflux of CO_2 from the cell, but at a cost of consuming reducing equivalents (NADPH or reduced Fd) (Price *et al.*, 2008). Despite having a mechanism for intracellular recycling of CO_2 , efflux is reported to account for the loss of up to 50% of HCO_3^- uptake in *Trichodesmium* (Eichner *et al.*, 2015; Kranz *et al.*, 2010).

As reviewed in Boatman *et al.* (2017), the majority of previous studies show an increase (albeit not all statistically significant) in *T. erythraeum* IMS101 growth to future CO_2 concentrations (~ 750/1000 $\mu\text{mol mol}^{-1}$). This mirrors the increased productivity (CO_2 and N_2 fixation) and changing elemental composition in response to future CO_2 concentrations (~ 750/1000 $\mu\text{mol mol}^{-1}$), although the magnitudes of these responses differs between studies (Table S1). The increased productivity of *T. erythraeum* IMS101 with increased CO_2 is likely

attributable to a decrease in the energy required for operation of the CCM, allowing more energy (ATP) and reductant (NADPH) to be reallocated to N₂ fixation, CO₂ fixation and biosynthesis (Kranz *et al.*, 2011).

Given *Trichodesmium*'s significant contribution to carbon and nitrogen biogeochemical cycles and the predicted changes to Ci speciation over the coming decades due to ocean acidification, we performed a systematic experiment to assess how the kinetics of Ci assimilation of *T. erythraeum* IMS101 were affected by acclimation to varying CO₂ concentrations ($\mu\text{mol mol}^{-1}$). We ensured that the Ci chemistry and all other growth conditions were well defined, with cultures fully acclimated over long-time periods to achieve balanced growth. We assessed how the rate of Ci assimilation was related to CO₂ or HCO₃⁻ concentrations in experiments where Ci speciation was modulated by varying pH and TIC. These assays of photosynthetic performance showed that i) *Trichodesmium* productivity was influenced by high-pH when TIC was held at a saturating concentration, indirectly making the rate of Ci assimilation a saturating function of CO₂ concentration and ii), maximum rates of CO₂ fixation declined and affinity for CO₂ increased when *Trichodesmium* was acclimated to a low-CO₂ concentration. We discuss how these responses can be attributed to decreases in the cost of operating a CCM at future CO₂ conditions.

Materials and methods

T. erythraeum IMS101 was semi-continuously cultured to achieve fully acclimated balanced growth at three target CO₂ concentrations (180, 380 and 720 $\mu\text{mol mol}^{-1}$), saturating light intensity (400 $\mu\text{mol photons m}^{-2} \text{s}^{-1}$), 12:12 light:dark (L:D) cycle and optimum growth temperature (26 °C \pm 0.7 °C) for ~ 5 months (~ 80 generations).

Experimental setup

T. erythraeum IMS101 was grown using YBCII medium (Chen *et al.*, 1996) at 1.5 L volumes in 2 L pyrex bottles that had been acid-washed and autoclaved prior to culturing. Daily growth rates were quantified from changes in baseline fluorescence (F_o) measured between 09:00 to 10:30 on dark-adapted cultures (20 minutes) using a FRRfII FastAct Fluorometer System (Chelsea Technologies Group Ltd, UK). Cultures were deemed fully acclimated and

in balanced growth when both the slope of the linear regression of $\ln F_o$ and the ratio of live cell to acetone extracted (method detailed below) baseline fluorescence (F_o) were constant following every dilution with fresh YBCII medium. Cultures were kept at the upper section of the exponential growth phase through periodic dilution with new growth media at 3 to 5 day intervals. Illumination was provided side-on by fluorescent tubes (Sylvania Luxline Plus FHQ49/T5/840). Cultures were constantly mixed using magnetic PTFE stirrer bars and aerated with a filtered (0.2 μ m pore) air mixture at a rate of $\sim 200 \text{ mL s}^{-1}$. The CO_2 concentration was regulated ($\pm 2 \mu\text{mol mol}^{-1}$) by mass flow controllers (Bronkhorst, Newmarket, UK) where CO_2 -free air was supplied by an oil free compressor (Bambi Air, UK) via a soda lime gas-tight column which was mixed with a 10% CO_2 in-air mixture from a gas cylinder (BOC Industrial Gases, UK). The CO_2 concentration in the gas phase was continuously monitored and recorded by an infra-red gas analyser (Li-Cor Li-820, Nebraska USA), calibrated weekly by a standard gas (BOC Industrial Gases).

The Ci chemistry was measured prior to the dilution of each culture with fresh media; where pH and TIC were measured directly, while the bicarbonate (HCO_3^-), carbonate (CO_3^{2-}) and CO_2 concentrations were calculated via *CO2SYS* using the same constants as described in Boatman *et al.* (2017) (Supplementary Information: I).

Elemental stoichiometry

Samples for elemental composition and CO_2 response curves were collected at the same time of day between 4 and 6 hours into the photo-phase of the L:D cycle. Samples for determination of particulate organic carbon (POC), particulate nitrogen (PN) and particulate phosphorus (PP) were collected with each CO_2 response curve, where each sample was a biological replicate culture. Three 100 mL aliquots from each culture were vacuum-filtered onto pre-combusted 25 mm (0.45 μ m pore) glass fibre filters for measurements of POC, PN and PP. The POC and PN filters were placed in 1.8 mL cryovials (lids off) and dried at 60 °C. The POP filters were rinsed with 2 mL of sodium sulphate (0.1 M), placed in a glass 20 mL scintillation vial, 2 mL of magnesium sulphate (0.017 M) added and dried at 60 °C. POC was quantified using a TC analyser (Shimadzu TOC-V Analyser & SSM-5000A Solid Sample Combustion Unit), PN by the method of Bronk and Ward (2000) and PP by the method of Solorzano and Sharp (1980).

Inorganic carbon fixation response curves

The dependencies of CO₂ fixation on CO₂ and HCO₃⁻ were obtained from experiments that involved (i) varied TIC with fixed pH and (ii) varied pH with fixed TIC (Supplementary Information: II and III) in TRIS-buffered YBCII medium using the ¹⁴C uptake technique (Nielsen and Jensen, 1957).

Prior to each experiment, 1 L of bicarbonate-free YBCII medium was aerated overnight with CO₂-free air (soda lime column). A 200 mL sample from each culture (triplicate cultures) was gravity filtered onto a cyclopore (1 µm pore) 47 mm filter (Whatman 60750) and gently re-suspended into 50 mL of CO₂-free YBCII medium. Exactly 5 mL of concentrated culture was pipetted into each tube of the TIC or pH gradients (35 mL total volume per tube) and gently inverted to evenly distribute the trichomes. The remaining culture was used for T₀ measurements, requiring an additional three test tubes (one per culture). During sample preparation, test tubes were maintained at growth temperature (26 °C) and a low light intensity (< 10 µmol photons m⁻² s⁻¹).

To characterise the C_i chemistry, exactly 20 mL of culture from each treatment was filtered through a swinnex filter (25 mm, 0.45µm pore, glass fibre filter); 15 mL into plastic centrifuge tube (no headspace) for TIC analysis (Shimadzu TOC-V Analyser & ASI-V Autosampler), and 5 mL into a plastic cryogenic vial (Sigma-Aldrich V5257-250EA) (no headspace) for pH analysis.

To measure chlorophyll *a* concentrations, a 1 mL sample from each treatment was pipetted into 9 mL of 100% acetone and left in the freezer (-20 °C) overnight (Welschmeyer, 1994). The sample was vortex mixed and left in the dark (~ 30 minutes) for cell debris to precipitate and the solution to equilibrate to room temperature. A 2 mL aliquot was used to measure baseline fluorescence (*F*₀) using a FRRfII FastAct Fluorometer System (Chelsea Technologies Group Ltd, UK) with the same parameters as live cultures. Chlorophyll *a* concentrations were calculated from a calibration curve derived from a dilution series measured on a chlorophyll *a* standard (Sigma-Aldrich C5753).

To assess whether cells had been affected by i), concentration via filtration and resuspension and ii), exposure to the range of TIC and pH gradients over the course of the ¹⁴C incubations, 2 mL aliquots of culture from each treatment were dark acclimated (~ 20 minutes) and the

photosynthetic efficiency of PSII (F_v/F_m) measured using a FRRfII FastAct Fluorometer System (Chelsea Technologies Group Ltd, UK) (Fig. S1).

Finally, 10 mL of culture from each treatment was pipetted into 12 mL glass (PTFE capped) test tubes and used for ^{14}C incubations. A ^{14}C spike solution was prepared by pipetting 45 μL of a ^{14}C labelled sodium bicarbonate solution ($\text{NaH}^{14}\text{CO}_3$) with a specific activity of 52 mCi mmol^{-1} (Perkin Elmer, USA) into 8 mL of bicarbonate-free YBCII media. Exactly 250 μL of the spike was added to each tube culture. The T_0 tubes were immediately filtered through swinnex filters containing (0.45 μm pore) 25mm diameter glass fibre filters and placed in scintillation vials and acidified (500 μL of 3 M HCl). To determine the total activity (TC), precisely 20 μL of the spike was added into three scintillation vials already containing 4.5 mL of scintillation cocktail (Gold LLT) and 200 μL of phenylethylamine. The TC vial caps were screwed tight immediately. The spiked test tubes were placed within a custom-made water-jacketed incubator and maintained at 26 $^\circ\text{C}$ and saturating light intensity ($400 \pm 6 \mu\text{mol photons m}^{-2} \text{s}^{-1}$) (The Optoelectronic Manufacturing Corporation Ltd. 1ft T5 Daylight, UK). The incubations lasted between 60 and 90 minutes and occurred between 4 to 6 hours into the photophase of the L:D cycle. The ^{14}C incubations were repeated in the dark, using black-coated (Plasti-Kote paint) test tubes. Dark ^{14}C uptake rates were 8.25% (± 0.46) and 7.05% (± 0.25) of the maximum light-saturated ^{14}C uptake rates for the TIC and pH response curves, respectively. Dark ^{14}C uptake rates exhibited no response to varying TIC or pH and were used to correct the light-dependent rates of photosynthesis (Li and Dickie, 1991).

To terminate ^{14}C uptake, samples were filtered through glass fibre (0.45 μm pore) 25 mm filters (Fisherbrand FB59451, UK) using a bespoke 30-funnel filtration manifold. Test tubes and filters were rinsed twice with 5 mL of YBCII media, before the filters were placed into scintillation vials. The vials were acidified (500 μL of 3 M HCl) overnight along with the T_0 samples. Exactly 4.5 mL of scintillation cocktail (Gold LLT) was added to the acidified vials and the caps tightened. Ensuring that the scintillation cocktail and filtered samples were well mixed, the vials were placed within a scintillation counter and the disintegrations per minute (DPM) of each vial measured (20 minutes per vial). The CO_2 fixation rates were calculated using the following equation;

$$C - fixation = \left(\frac{DPM_{(S)} - DPM_{(T_0)}}{DPM_{(TC)}} \right) \cdot \left(\frac{V_{(TC)}}{V_{(S)}} \right) \cdot \left(\frac{[TCO_2]}{t} \right) \cdot 1.05 \quad (1)$$

where the disintegrations per minute (DPM) were measured for the sample (S), initial (T_0) and total activity (TC) vials; TIC (mmol L^{-1}) is the mean concentration of TIC within the sample over the course of the incubation (inclusive of the $\text{NaH}^{14}\text{CO}_3$ spike); $V_{(\text{TC})}$ and $V_{(\text{S})}$ are the volumes of the sample and TC vials, respectively; t is the experimental incubation time (h^{-1}); and 1.05 is a radioisotope discrimination factor ($^{12}\text{C}:^{14}\text{C}$). Note that mean T_0 and TC values were used when calculating the C-fixation rates ($n = 3$).

Inorganic carbon fixation rates were normalised to a POC basis and the CO_2 response curves fitted to a Michaelis-Menten function;

$$V^C = \frac{(V_m^C \cdot \text{CO}_2)}{(K_m + \text{CO}_2)} \quad (2)$$

where V^C is the organic C-specific rate of CO_2 fixation, V_m^C is the maximum rate of CO_2 fixation and K_m is the half saturation constant. Curve fitting was performed on individual replicates to calculate mean (\pm S.E.) curve fit parameterisations (Sigmaplot 11.0), as well on the combined data where all replicates of the varied TIC (fixed pH) and varied pH (fixed TIC) data was combined per CO_2 treatment.

Spectrophotometric chlorophyll a analysis

Samples for spectrophotometric determination of chlorophyll *a* were collected with each CO_2 response curve and were used to normalise productivity rates as well as to calculate Chl *a*:C. A 100 mL sample from each culture was vacuum-filtered onto a 25 mm (0.45 μm pore) glass fiber filter (Fisherbrand FB59451, UK) and extracted in 5 mL of 100% methanol. Filters were homogenised and extracted overnight at -20°C , before being centrifuged at 10,000 rpm for 10 minutes and a 3 mL aliquot of the supernatant added to a quartz cuvette. The absorption spectrum (400 to 800 nm) was measured using a (Hitachi U-3000, Japan) spectrophotometer and the Chl *a* concentration ($\mu\text{g L}^{-1}$) calculated using the following equation (Ritchie, 2008);

$$\text{Chl } a = \left[\frac{(12.9447 \cdot (\text{Abs}^{665} - \text{Abs}^{750})) \cdot V_{(\text{E})}}{V_{(\text{F})}} \right] \cdot 1000 \quad (3)$$

where Abs^{665} and Abs^{750} are the baseline-corrected optical densities of the methanol extracted sample at 665 and 750 nm; $V_{(\text{E})}$ is the volume of the solvent used for extraction (i.e. 5 mL);

$V_{(F)}$ is the volume of culture filtered (i.e. 100 mL); and 12.9447 is a cyanobacteria-specific Chl *a* coefficient for 100% methanol extraction.

Modelling the CCM

The CO_2 and HCO_3^- fluxes and concentrations in an idealised *Trichodesmium* cell were calculated using the numerical model from Mangan *et al.* (2016) and Mangan and Brenner (2014). The aim was to offer a qualitatively informative view of the CCM system, without attempting to match carboxylation rates or fluxes to the experimental system or rescale the results from the idealised cell to what would be expected from the experimental data. With the exception of a few key parameter values (Table 2), the model is equivalent to that reported in Mangan *et al.* (2016). The main changes between the idealised *Trichodesmium* cell and previous models are the increase in cell and carboxysome size to be consistent with reported values for *T. erythraeum*, changing the RuBisCO kinetic constants, using pH and external CO_2 and HCO_3^- concentrations similar to those in the ^{14}C incubations, updating the $\text{pK}_{a_{\text{eff}}}$ for HCO_3^- to CO_2 to match that used in the *CO2SYS* calculation and re-calculating the HCO_3^- uptake rate to support internal inorganic carbon concentrations of ~ 30 mM. We scaled the RuBisCO concentration by the carboxysome volume, so that the activity per volume remained the same. Similarly, we scaled the amount of carbonic anhydrase by the carboxysome surface area, so that the activity per area remained the same. The carbonic anhydrase activity was sufficient to equilibrate CO_2 and HCO_3^- to $K'_{\text{eq}} = \frac{[\text{HCO}_3^-]}{[\text{CO}_2]} = 10^{-\text{pK}_{\text{eff}} + \text{pH}}$. We set the carbonic anhydrase K_{ca} value to preserve the correct equilibrium value for the internal pH.

Results

Inorganic carbon chemistry, growth rate and cell composition

Overall the CO_2 drawdown in the cultures ranged between 57 to 78 $\mu\text{mol mol}^{-1}$ for all CO_2 treatments (Table 1) and exhibited a negligible CO_2 drift over a diurnal cycle (Fig. S2). Dissolved inorganic NH_4^+ concentrations in the growth medium were ~ 1 μM , while NO_3^- concentrations were ~ 0.3 μM , which is below the 1 μM detection limit.

Balanced growth rates increased from $\sim 0.2 \text{ d}^{-1}$ at low- CO_2 to $\sim 0.34 \text{ d}^{-1}$ at mid- CO_2 and $\sim 0.36 \text{ d}^{-1}$ at high- CO_2 (Table 3). The dark adapted photochemical efficiencies of PSII (F_v/F_m) were proportionate to the growth CO_2 , increasing from 0.27 at low- CO_2 to ~ 0.31 at mid- CO_2 and ~ 0.34 at high- CO_2 (Table 3). The particulate C:N ratio was independent of CO_2 , while the C:P and N:P ratios increased with increasing CO_2 (Table 3). Both Chl *a*:C and Chl *a*:N ratios were about 30-40% higher at mid- CO_2 than at low or high- CO_2 .

CO₂ response curves

Based on shape of the response curves, inorganic carbon (^{14}C) fixation rate was fit to a saturating function of the dissolved CO_2 concentration in both the pH gradient and TIC gradient experiments (Fig. 1). Although a saturating function of HCO_3^- concentration was observed when TIC was varied at constant pH (Fig. 1A-C), C_i assimilation could not be described by the same kinetic constants when pH was varied at constant TIC (Fig. 1D-F).

The K_m for photosynthetic C-fixation increased from $0.8 \mu\text{M}$ in cultures acclimated to a low- CO_2 to $2.2 \mu\text{M}$ and $3.2 \mu\text{M}$ in cultures acclimated to mid and high- CO_2 , respectively and were approximately 4 to 5-fold lower than the ambient CO_2 concentrations in the cultures. The maximum organic carbon specific rate of C-fixation (V_m^C) was also higher in cells grown at mid- CO_2 than at low- CO_2 , although the rates at mid and high- CO_2 did not differ significantly (Table 4). The affinity for CO_2 (V_m^C/K_m) declined by about 40% with increasing CO_2 (Table 4).

Modelled response curves

Without parameter fitting, the model of *Trichodesmium's* CCM produced behaviors consistent with the experimental data when either external TIC (i.e HCO_3^-) was varied at a fixed pH or when pH was varied at a fixed TIC (Fig. 2A,B). Assuming HCO_3^- is the dominant form of inorganic carbon taken up by the cell (Eichner *et al.*, 2015; Kranz *et al.*, 2009), *Trichodesmium* exhibited a significant response to changes in external pH and CO_2 concentrations. The decrease in carboxylation rate with decreasing external CO_2 was due to a decrease in HCO_3^- uptake (when TIC was varied) or an increase in HCO_3^- and CO_2 leakage out of the cell (when pH was varied) (Fig. S3). Modelled carboxylation rates from both

numerical simulations exhibited a smooth function of HCO_3^- uptake, HCO_3^- leakage and CO_2 leakage (Fig. 2C).

The V_m^C of the pH gradient and TIC gradient experiments were not significantly different (Table S3). However, the maximum carboxylation rates from the simulations were significantly different (Fig. 2); principally because the external HCO_3^- concentration used in the pH-dependent simulation (chosen to be the same as the experiment) was not sufficient to saturate RuBisCO. It is possible that the K_m assumed for RuBisCO was set too high, or the internal pH, geometry, or HCO_3^- uptake values are substantially different. Note that we are simulating values beyond the range of those in the experiments, so such a discrepancy is magnified.

Discussion

Amongst our key findings are: (i) The acclimated growth rate increased from low- to mid- CO_2 but did not increase significantly between mid- and high- CO_2 treatments, suggesting that the positive effect of elevated CO_2 on *Trichodesmium* carbon assimilation over the coming decades may only be slight. (ii) The maximum rate (V_m^C) and the half saturation constant (K_m) for C-fixation increased with growth CO_2 , but the affinity for CO_2 (V_m^C/K_m) declined, which is likely attributed to *Trichodesmium*'s CCM activity. (iii) Measured inorganic C-fixation rate in *Trichodesmium* could be described as a saturating function of CO_2 both when CO_2 was manipulated by varying pH at constant TIC and when CO_2 was manipulated by varying TIC at constant pH. (iv) A mechanistic model of *Trichodesmium*'s CCM indicates that the former is due to HCO_3^- uptake limitation of carboxylation rate, whereas the latter is due to a high-pH mediated increase in HCO_3^- and CO_2 leakage, potentially coupled to other unknown processes operating outside of the paratermised model that are restricting Ci assimilation rates at high-pH. Such processes may involve the direct effect of pH on membrane conformation, membrane transport processes or metabolic functions.

Effect of acclimation to variation of inorganic chemistry on growth rates and elemental stoichiometry

Increased growth rate from low- ($180 \mu\text{mol mol}^{-1}$) to mid- ($380 \mu\text{mol mol}^{-1}$) and high- CO_2 ($720 \mu\text{mol mol}^{-1}$) was similar to previous findings (Barcelos e Ramos *et al.*, 2007; Boatman *et al.*, 2017). Growth rate at high CO_2 was 8% greater than at mid- CO_2 , but this difference was not statistically significant. The magnitude of this increase at high CO_2 is comparable to several recent studies, which report growth rate increases of between 7 to 26% with increases of CO_2 beyond $400 \mu\text{mol mol}^{-1}$ (Barcelos e Ramos *et al.*, 2007; Boatman *et al.*, 2017; Garcia *et al.*, 2011; Hutchins *et al.*, 2007; Kranz *et al.*, 2010; Levitan *et al.*, 2007).

The observed increase in C:P and N:P are consistent with previous findings (Barcelos e Ramos *et al.*, 2007; Kranz *et al.*, 2010; Levitan *et al.*, 2010), where changes can be ascribed to increases in cellular N and C incorporation, with P quotas relatively unaffected by CO_2 (Hutchins *et al.*, 2007; Kranz *et al.*, 2010). In contrast, the C:N and thus the balance between CO_2 fixation and N_2 fixation was not significantly affected by the growth CO_2 . Similarly, Levitan *et al.* (2007) found C:N varied only slightly (from 6.5 to 7.0) across growth CO_2 concentrations from 250 to $900 \mu\text{mol mol}^{-1}$.

We report C-specific rates here as these are most directly related to changes in specific growth rate because both rates can be expressed in equivalent units of inverse time (e.g. h^{-1} or d^{-1}). However, we note that due to differences in the Chl *a*:C ratio, chlorophyll *a*-specific rates showed a different pattern, increasing progressively from low- through mid- to high- CO_2 (Table S2, Fig. S4). A reduction in Chl *a*:C decreases the energy demands associated with synthesis of the photosynthetic apparatus and is dictated by the total demands for reductant (NADPH) and high-energy phosphate bonds (ATP) (Geider *et al.*, 2009), the minimum turnover times for PSII (τ_{PII}) and PSI (τ_{PI}) and the minimum pigment content required for effective light absorption and energy transfer (a_{min}) (Behrenfeld *et al.*, 2008). We suggest that the reduced Chl *a*:C at low CO_2 relative to mid CO_2 is likely due to the cost of up-regulating the CCM, whereas the reduced Chl *a*:C at high CO_2 may be due to an increase in carbohydrate storage granules relative to the mid CO_2 treatment (Table 3).

CO₂ response curves

Growth rates reported here are comparable to the 2 μM EDTA, iron replete (unchelated) treatments in Boatman *et al.* (2017), as well as 20 μM EDTA, iron replete (chelated) cultures (Boatman *et al.*, Unpublished); suggesting that cultures were not exposed to toxic concentrations of certain trace metals (e.g. copper) caused from low trace metal buffering capacity as reported by Hong *et al.* (2017). Furthermore, dissolved inorganic NH_4^+ concentrations were consistently around 0.3 μM (Table 1). We are therefore confident that the observed positive effect of ocean acidification on growth and primary productivity is driven by the increased CO_2 concentration, rather than a consequence of a pH induced shift of the $\text{NH}_3/\text{NH}_4^+$ equilibrium. We measured CO_2 response curves at one time of day (4 to 6 hours into the photo-phase of a 12:12 L:D cycle) and as such cannot extrapolate to a diel response given the reports of temporal separation of photosynthesis and N_2 fixation in *Trichodesmium* (Berman-Frank *et al.*, 2001).

The mechanistic model of Mangan *et al.* (2016) indicates that the CO_2 response we observed when the TIC was varied (pH fixed) was caused by HCO_3^- limitation, where HCO_3^- uptake limits the rate of carboxylation. Conversely, the CO_2 response we observed when pH was varied (TIC fixed) is a function of the pH dependency of HCO_3^- and CO_2 leakage, which in turn could lead to CO_2 limitation of C-fixation and/or diversion of reducing equivalents from powering CO_2 fixation via the Calvin cycle to powering the conversion of CO_2 to HCO_3^- by the NDH-I₄ complex. The model of *Trichodesmium*'s CCM shows the relative importance of leakage, which is notably sensitive to certain parameters in the system such as internal pH, RuBisCO activity, cell size and carboxysome size.

Previous studies have shown a notable response in CCM activity to changes in CO_2 ; for example a two-fold lower DIC half saturation concentration in cells acclimated to 150 $\mu\text{mol mol}^{-1}$ (pH_{NBS} 8.56) compared with 370 $\mu\text{mol mol}^{-1}$ (pH_{NBS} 8.26) (Kranz *et al.*, 2009). Our experimental observations indicate that Ci assimilation (V^{C}) is well described by a CO_2 response curve, but not by a single HCO_3^- response curve (Fig. 1). Here we offer an explanation as to the response of V^{C} to HCO_3^- concentration in the experiments where we varied $\text{pH}_{(\text{Total})}$ from 7.65 to 8.5 at constant TIC.

Based on the numerical simulations, carboxylation rates across an external pH gradient ranging from 7.5 to 8.5 exhibit a clear linear response, which cannot be ascribed to a Michaelis-Menten function (Fig. S3). Conversely, our experimental data shows a clear and

significant decrease in Ci assimilation rates at low external CO₂/high-pH (Fig. 1). In addition, the Ci assimilation rates for the pH gradient and TIC gradient experiments, for all replicates of all three CO₂ treatments, exhibited similar inflection points to external CO₂ (Fig. S5). In order for the simulated system to exhibit a rate saturating response to external CO₂, CO₂ would have to be the dominant source of inorganic carbon. This would contradict all previous research showing that HCO₃⁻ accounts for > 90% of inorganic carbon uptake (Kranz *et al.*, 2009; Kranz *et al.*, 2010) and with the currently accepted mechanism of Ci assimilation in *T. erythraeum* IMS101 (Badger and Price, 2003).

Given how well the numerical simulations modelled carboxylation rates as a smooth function of HCO₃⁻ uptake, HCO₃⁻ leakage and CO₂ leakage (Fig. 2C), we propose that the linear pH-dependency on carboxylation rate predicted by the model is mechanistically correct, but that processes not captured by the model are contributing to the decrease in Ci assimilation rate at high-pH. Such factors could include a direct effect of high-pH on cell membrane properties and alteration in membrane conformation (Myklestad and Swift, 1998), or the influence of pH on membrane transport processes and metabolic functions involved in cellular pH regulation (Raven, 1981).

Interestingly, for the mid and high CO₂ treatments, a Michaelis-Menten function provided a better fit for the pH varied (TIC fixed) data than a linear regression. However, there was no significant difference between a linear or Michaelis-Menten function for the low CO₂ data, which suggests that full acclimation to a high-pH environment prior to the ¹⁴C incubations lessened the negative effect that high-pH had on Ci assimilation.

Based on our simulation, *Trichodesmium*'s actual carboxylation rate should be modelled as a function of HCO₃⁻ and pH. This is because the CO₂ concentration in a saturated HCO₃⁻/high-pH (i.e. 3.8 mM HCO₃⁻, pH = 8.4) environment could be equivalent to a limited HCO₃⁻/present pH (i.e. 1.9 mM HCO₃⁻, pH = 8.1) environment; which for the aforementioned reasons, will impose different constraints on leakage/uptake rates. That said, our experimental data clearly suggests that high-pH induced processes operating outside of the CCM are contributing to decrease Ci assimilation. Overall, this may allow *Trichodesmium*'s Ci assimilation rates to be ascribed as a function of CO₂ (Fig. 1, Fig. S4), which would be considerably simpler to implement in biogeochemical models of *Trichodesmium* growth and photosynthesis (Hutchins *et al.*, 2013) than a HCO₃⁻ response curve in which the kinetic constants (K_m and V_m) are pH-dependent. Further experimental work is needed to assess

whether a CO₂ parameterisation is consistent across an extended range of pH and HCO₃⁻ conditions than those used in our experiments.

Conclusion

Climate change is driving ocean acidification, which results in higher CO₂ and HCO₃⁻ concentrations and a decrease in pH. We observed systematic changes in the kinetics of inorganic carbon assimilation of *T. erythraeum* IMS101 in response to acclimation to CO₂ ranging from low-CO₂ (levels at the last glacial maximum) through mid-CO₂ (levels at the end of the 20th century) to high-CO₂ (levels predicted for 2050 to 2100). Extrapolating these responses to future scenarios of the natural environment should consider i), these findings were obtained using acclimation experiments whereas *Trichodesmium* may adapt to future conditions (Hutchins *et al.*, 2015); ii), variability may exist between strains and clades (Hutchins *et al.*, 2013); and iii), the additional effects of integrated abiotic variables (i.e. light and temperature) and nutrients (i.e. P and Fe) on *Trichodesmium* productivity (Walworth *et al.*, 2016).

In the context of the open-oceans, our results indicate that nutrient-replete net photosynthesis and growth rates of *T. erythraeum* IMS101 would have been severely CO₂ limited at the last glacial maximum relative to current conditions. However, future increases in CO₂ (i.e. 720 μmol mol⁻¹) may not significantly increase growth and productivity of IMS101, although we note that others report a stimulation of growth and photosynthesis by increasing CO₂ beyond current ambient concentrations (Hutchins *et al.*, 2007; Levitan *et al.*, 2010; Levitan *et al.*, 2007). However, we did observe that growth under high CO₂ will increase key stoichiometric ratios (N:P and C:P). Increases of N:P and C:P in *Trichodesmium*-dominated oceanic regimes may affect bacterial and zooplankton metabolism, the pool of bioavailable nitrogen, the depth at which sinking organic matter is remineralised and consequently carbon sequestration via the biological carbon pump (McGillicuddy, 2014; Mulholland *et al.*, 2004). These responses could serve as a negative feedback to climate change by increasing new N and C production and thereby increasing the organic carbon sinking to the deep ocean.

Acknowledgements

Tobias Boatman was supported by a UK Natural Environment Research Council PhD studentship (NE/J500379/1 DTB).

Accepted Manuscript

References

- Badger M, Andrews T.** 1987. Co-evolution of Rubisco and CO₂ concentrating mechanisms. *Progress in Photosynthesis Research*: Springer, 601-609.
- Badger MR, Andrews TJ, Whitney S, Ludwig M, Yellowlees DC, Leggat W, Price GD.** 1998. The diversity and coevolution of Rubisco, plastids, pyrenoids, and chloroplast-based CO₂-concentrating mechanisms in algae. *Canadian Journal of Botany* **76**, 1052-1071.
- Badger MR, Hanson D, Price GD.** 2002. Evolution and diversity of CO₂ concentrating mechanisms in cyanobacteria. *Functional Plant Biology* **29**, 161-173.
- Badger MR, Palmqvist K, Yu JW.** 1994. Measurement of CO₂ and HCO₃⁻ fluxes in cyanobacteria and microalgae during steady-state photosynthesis. *Physiologia Plantarum* **90**, 529-536.
- Badger MR, Price GD.** 2003. CO₂ concentrating mechanisms in cyanobacteria: molecular components, their diversity and evolution. *Journal of Experimental Botany* **54**, 609-622.
- Badger MR, Price GD, Long BM, Woodger FJ.** 2006. The environmental plasticity and ecological genomics of the cyanobacterial CO₂ concentrating mechanism. *Journal of Experimental Botany* **57**, 249-265.
- Barcelos e Ramos J, Biswas H, Schulz KG, LaRoche J, Riebesell U.** 2007. Effect of rising atmospheric carbon dioxide on the marine nitrogen fixer *Trichodesmium*. *Global biogeochemical cycles* **21**, GB2028.
- Behrenfeld MJ, Halsey KH, Milligan AJ.** 2008. Evolved physiological responses of phytoplankton to their integrated growth environment. *Philosophical Transactions of the Royal Society B: Biological Sciences* **363**, 2687-2703.
- Berman-Frank I, Lundgren P, Chen YB, Küpper H, Kolber Z, Bergman B, Falkowski PG.** 2001. Segregation of nitrogen fixation and oxygenic photosynthesis in the marine cyanobacterium *Trichodesmium*. *Science* **294**, 1534-1537.
- Boatman TG, Lawson T, Geider RJ.** 2017. A Key Marine Diazotroph in a Changing Ocean: The Interacting Effects of Temperature, CO₂ and Light on the Growth of *Trichodesmium erythraeum* IMS101. *PLoS One* **12**, e0168796.
- Bronk DA, Ward BB.** 2000. Magnitude of dissolved organic nitrogen release relative to gross nitrogen uptake in marine systems. *Limnology and Oceanography* **45**, 1879-1883.
- Capone DG, Burns JA, Montoya JP, Subramaniam A, Mahaffey C, Gunderson T, Michaels AF, Carpenter EJ.** 2005. Nitrogen fixation by *Trichodesmium* spp.: An important source of new nitrogen to the tropical and subtropical North Atlantic Ocean. *Global biogeochemical cycles* **19**, GB2024.
- Chen YB, Zehr JP, Mellon M.** 1996. Growth and nitrogen fixation of the diazotrophic filamentous nonheterocystous cyanobacterium *Trichodesmium* Sp. IMS 101 in defined media: evidence for a circadian rhythm. *Journal of Phycology* **32**, 916-923.
- Collos Y, Mornet F, Sciandra A, Waser N, Larson A, Harrison P.** 1999. An optical method for the rapid measurement of micromolar concentrations of nitrate in marine phytoplankton cultures. *Journal of Applied Phycology* **11**, 179-184.
- Davis CS, McGillicuddy DJ.** 2006. Transatlantic abundance of the N₂-Fixing colonial cyanobacterium *Trichodesmium*. *Science* **312**, 1517-1520.
- Eichner M, Thoms S, Kranz SA, Rost B.** 2015. Cellular inorganic carbon fluxes in *Trichodesmium*: a combined approach using measurements and modelling. *Journal of Experimental Botany* **66**, 749-759.
- Garcia NS, Fu F-X, Breene CL, Bernhardt PW, Mulholland MR, Sohm JA, Hutchins DA.** 2011. Interactive effects of Irradiance and CO₂ on CO₂ fixation and N₂ fixation in the Diazotroph *Trichodesmium erythraeum* (Cyanobacteria). *Journal of Phycology* **47**, 1292-1303.
- Geider RJ, Moore CM, Ross ON.** 2009. The role of cost-benefit analysis in models of phytoplankton growth and acclimation. *Plant Ecology and Diversity* **2**, 165-178.

- Hong H, Shen R, Zhang F, Wen Z, Chang S, Lin W, Kranz SA, Luo Y-W, Kao S-J, Morel FM.** 2017. The complex effects of ocean acidification on the prominent N₂-fixing cyanobacterium *Trichodesmium*. *Science* **356**, 527-531.
- Hutchins D, Fu FX, Zhang Y, Warner M, Feng Y, Portune K, Bernhardt P, Mulholland M.** 2007. CO₂ control of *Trichodesmium* N₂ fixation, photosynthesis, growth rates, and elemental ratios: implications for past, present, and future ocean biogeochemistry. *Limnology and Oceanography* **52**, 1293-1304.
- Hutchins DA, Fu F-X, Webb EA, Walworth N, Tagliabue A.** 2013. Taxon-specific response of marine nitrogen fixers to elevated carbon dioxide concentrations. *Nature Geoscience* **6**, 790-795.
- Hutchins DA, Walworth NG, Webb EA, Saito MA, Moran D, McIlvin MR, Gale J, Fu F-X.** 2015. Irreversibly increased nitrogen fixation in *Trichodesmium* experimentally adapted to elevated carbon dioxide. *Nature communications* **6**, 8155.
- Kaplan A, Reinhold L.** 1999. CO₂ concentrating mechanisms in photosynthetic microorganisms. *Annual review of plant biology* **50**, 539-570.
- Kranz S, Eichner M, Rost B.** 2011. Interactions between CCM and N₂ fixation in *Trichodesmium*. *Photosynthesis research* **109**, 73-84.
- Kranz S, Sültemeyer D, Richter KU, Rost B.** 2009. Carbon acquisition in *Trichodesmium*: The effect of pCO₂ and diurnal changes. *Limnology and Oceanography* **54**, 548-559.
- Kranz SA, Levitan O, Richter KU, Prášil O, Berman-Frank I, Rost B.** 2010. Combined effects of CO₂ and light on the N₂-fixing cyanobacterium *Trichodesmium* IMS101: physiological responses. *Plant physiology* **154**, 334-345.
- Levitan O, Brown CM, Sudhaus S, Campbell D, LaRoche J, Berman-Frank I.** 2010. Regulation of nitrogen metabolism in the marine diazotroph *Trichodesmium* IMS101 under varying temperatures and atmospheric CO₂ concentrations. *Environmental Microbiology* **12**, 1899-1912.
- Levitan O, Rosenberg G, Setlik I, Setlikova E, Grigel J, Klepetar J, Prasil O, Berman-Frank I.** 2007. Elevated CO₂ enhances nitrogen fixation and growth in the marine cyanobacterium *Trichodesmium*. *Global Change Biology* **13**, 531-538.
- Li W, Dickie P.** 1991. Light and dark ¹⁴C uptake in dimly-lit oligotrophic waters: relation to bacterial activity. *Journal of plankton research* **13**, 29-44.
- Mangan NM, Brenner MP.** 2014. Systems analysis of the CO₂ concentrating mechanism in cyanobacteria. *Elife* **3**, e02043.
- Mangan NM, Flamholz A, Hood RD, Milo R, Savage DF.** 2016. pH determines the energetic efficiency of the cyanobacterial CO₂ concentrating mechanism. *Proceedings of the National Academy of Sciences* **113**, E5354-E5362.
- McGillicuddy DJ.** 2014. Do *Trichodesmium* spp. populations in the North Atlantic export most of the nitrogen they fix? *Global biogeochemical cycles* **28**, 103-114.
- Mulholland MR, Bronk DA, Capone DG.** 2004. Dinitrogen fixation and release of ammonium and dissolved organic nitrogen by *Trichodesmium* IMS101. *Aquatic Microbial Ecology* **37**, 85-94.
- Mykkestad S, Swift E.** 1998. A new method for measuring soluble cellular organic content and a membrane property, T_m, of planktonic algae. *European Journal of Phycology* **33**, 333-336.
- Nielsen ES, Jensen EA.** 1957. Primary oceanic production. *The autotrophic production of organic matter in the oceans*, Vol. 1, 49-135.
- Price GD, Badger MR, Woodger FJ, Long BM.** 2008. Advances in understanding the cyanobacterial CO₂-concentrating-mechanism (CCM): functional components, C_i transporters, diversity, genetic regulation and prospects for engineering into plants. *Journal of Experimental Botany* **59**, 1441-1461.
- Raven J.** 1981. Nutrient transport in microalgae. *Advances in microbial physiology* **21**, 47-226.
- Raven J, Caldeira K, Elderfield H, Hoegh-Guldberg O, Liss P, Riebesell U, Shepherd J, Turley C, Watson A.** 2005. Ocean acidification due to increasing atmospheric carbon dioxide. The Royal Society of London.
- Ritchie R.** 2008. Universal chlorophyll equations for estimating chlorophylls a, b, c, and d and total chlorophylls in natural assemblages of photosynthetic organisms using acetone, methanol, or ethanol solvents. *Photosynthetica* **46**, 115-126.

- Schwarz R, Reinhold L, Kaplan A.** 1995. Low activation state of ribulose-1, 5-bisphosphate carboxylase/oxygenase in carboxysome-defective *Synechococcus* mutants. *Plant physiology* **108**, 183-190.
- Solorzano L.** 1969. Determination of ammonia in natural waters by the phenol hypochlorite method. *Limnology and Oceanography* **14**, 799-801.
- Solorzano L, Sharp JH.** 1980. Determination of total dissolved phosphorus and particulate phosphorus in natural waters. *Limnology and Oceanography* **25**, 754-758.
- Walworth NG, Fu F-X, Webb EA, Saito MA, Moran D, McIlvin MR, Lee MD, Hutchins DA.** 2016. Mechanisms of increased *Trichodesmium* fitness under iron and phosphorus co-limitation in the present and future ocean. *Nature communications* **7**.
- Welschmeyer NA.** 1994. Fluorometric analysis of chlorophyll *a* in the presence of chlorophyll *b* and pheopigments. *Limnology and Oceanography* **39**, 1985-1992.
- Zeebe RE, Wolf-Gladrow D, Jansen H.** 1999. On the time required to establish chemical and isotopic equilibrium in the carbon dioxide system in seawater. *Marine Chemistry* **65**, 135-153.
- Zeebe RE, Wolf-Gladrow DA.** 2001. *CO₂ in seawater: equilibrium, kinetics, isotopes*: Elsevier Science.

Accepted Manuscript

Table 1. The growth conditions (\pm S.E.) achieved for *T. erythraeum* IMS101 when cultured at three target gas phase CO_2 concentrations (Low = $180 \mu\text{mol mol}^{-1}$, Mid = $380 \mu\text{mol mol}^{-1}$ and High = $720 \mu\text{mol mol}^{-1}$), saturating light intensity ($400 \mu\text{mol photons m}^{-2} \text{s}^{-1}$) and optimal temperature (26°C).

Variables	Units	Low CO_2	Mid CO_2	High CO_2
pH	Total	8.458	8.174	7.906
H^+	nM	3.5 (0.20)	6.7 (0.13)	12.4 (0.28)
A_T	μM	2431 (70)	2447 (54)	2442 (56)
TIC	μM	1800 (69)	2039 (46)	2201 (50)
HCO_3^-	μM	1362 (67)	1743 (39)	2005 (44)
CO_3^{2-}	μM	435 (16)	289 (9)	179 (6)
CO_2	μM	3.3 (0.3)	8.1 (0.2)	17.3 (0.5)
NH_4^+	μM	1.03 (0.14)	1.00 (0.08)	1.08 (0.06)
NO_3^-	μM	0.34 (0.05)	0.32 (0.03)	0.30 (0.02)
<i>n</i>		89	67	39

Individual pH values were converted to a H^+ concentration, allowing a mean pH value to be calculated. Dissolved inorganic NH_4^+ was determined using the phenol-hypochlorite method as described by Solorzano (1969), while dissolved inorganic NO_3^- was determined using the spectrophotometric method as described by Collos *et al.* (1999).

Table 2. Key parameter values used in the numerical simulation of *Trichodesmium*'s CCM.

Variables	Units	Model Value
Cell radius, R_b	μm	3
Carboxysome radius R_c	μm	0.15
RuBisCO reaction rate k_{Rub}	1/s per active site	1.92
RuBisCO K_{CO_2}	μM	145
RuBisCO K_{O_2}	μM	600
RuBisCO specificity, S	-	45
Number of RuBisCO active sites	-	54000
Number of carbonic anhydrase active sites	-	900
Carbonic anhydrase $\frac{1}{2}$ max constant for CO_2 , K_{ca}	μM	104.7
Internal pH	-	8.3
$\text{pK}_{\text{a,eff}}$ for $\text{HCO}_3^-:\text{CO}_2$	-	5.84
Carboxysome permeability	cm/s	$3 \cdot 10^{-5}$
HCO_3^- uptake velocity, j_c	cm/s	$2.4 \cdot 10^{-7}$
CO_2 to HCO_3^- conversion at membrane	cm/s	$0.6 \cdot 10^{-7}$

The cell radius was measured from a bioimage collected using fluorescence microscopy (Fig. S12). Kinetic constants of RuBisCO carboxylation (K_{CO_2}), oxygenation (K_{O_2}) and the specificity factor (S) for a form 1B cyanobacteria were abstracted from Badger *et al.* (1998).

Table 3. The mean (\pm S.E.) balanced growth rate, dark adapted photochemical efficiency of PSII (F_v/F_m), elemental stoichiometry and chlorophyll a to C and N ratios for *T. erythraeum* IMS101 when acclimated to three target CO₂ concentrations (Low = 180 $\mu\text{mol mol}^{-1}$, Mid = 380 $\mu\text{mol mol}^{-1}$ and High = 720 $\mu\text{mol mol}^{-1}$), saturating light intensity (400 $\mu\text{mol photons m}^{-2} \text{s}^{-1}$) and optimal temperature (26 °C).

Variables	Units	Low CO ₂	Mid CO ₂	High CO ₂
Growth rate	d ⁻¹	0.198 (0.027) [A]	0.336 (0.026) [B]	0.361 (0.020) [B]
F_v/F_m	dimensionless	0.274 (0.025) [A]	0.305(0.020) [B]	0.342 (0.037) [C]
Elemental Stoichiometry				
C:N	mol:mol	7.9 (0.8)	7.8 (0.3)	7.3 (0.8)
C:P	mol:mol	91.9 (6.3) [A]	143.6 (6.3) [B]	155.5 (13.5) [B]
N:P	mol:mol	11.9 (0.6) [A]	18.4 (0.7) [B]	21.8 (1.7) [B]
Chl a:C	g:mol	0.052 (0.003) [A]	0.089 (0.003) [C]	0.066 (0.003) [B]
Chl a:N	g:mol	0.401 (0.037) [A]	0.693 (0.035) [B]	0.474 (0.043) [A]

Abbreviations; C:N, C:P and N:P ratios are mol:mol, Chl a:C and Chl a:N ratios are g:mol ($n = 9$ at low-CO₂, $n = 6$ at mid- and high-CO₂). Letters in parenthesis indicate significant differences between CO₂ treatments (One Way ANOVA, Tukey post hoc test; $P < .05$); where [B] is significantly greater than [A] and [C] is significantly greater than [B] and [A].

Accepted Manuscript

Table 4. The physiological parameters (\pm S.E.) of the C-specific C-fixation versus CO_2 concentration response curves for *T. erythraeum* IMS101. Data was fitted using the Michaelis-Menten model to obtain estimates of the half saturation constant (K_m) and maximum uptake rate (V_m^C) for CO_2 assimilation using the combined data from all replicates from both experiments employing varied TIC at fixed pH and varied pH at fixed TIC for each CO_2 treatment.

Parameters	Units	Low CO_2	Mid CO_2	High CO_2
V_m^C	h^{-1}	0.011 (0.0002)	0.024 (0.0007)	0.026 (0.0008)
K_m^C	$\mu\text{M CO}_2$	0.8 (0.1)	2.2 (0.3)	3.2 (0.4)
Affinity ^C	$\text{mM (CO}_2\text{)}^{-1} \text{h}^{-1}$	13.3 (1.7)	10.9 (1.5)	8.0 (1.0)

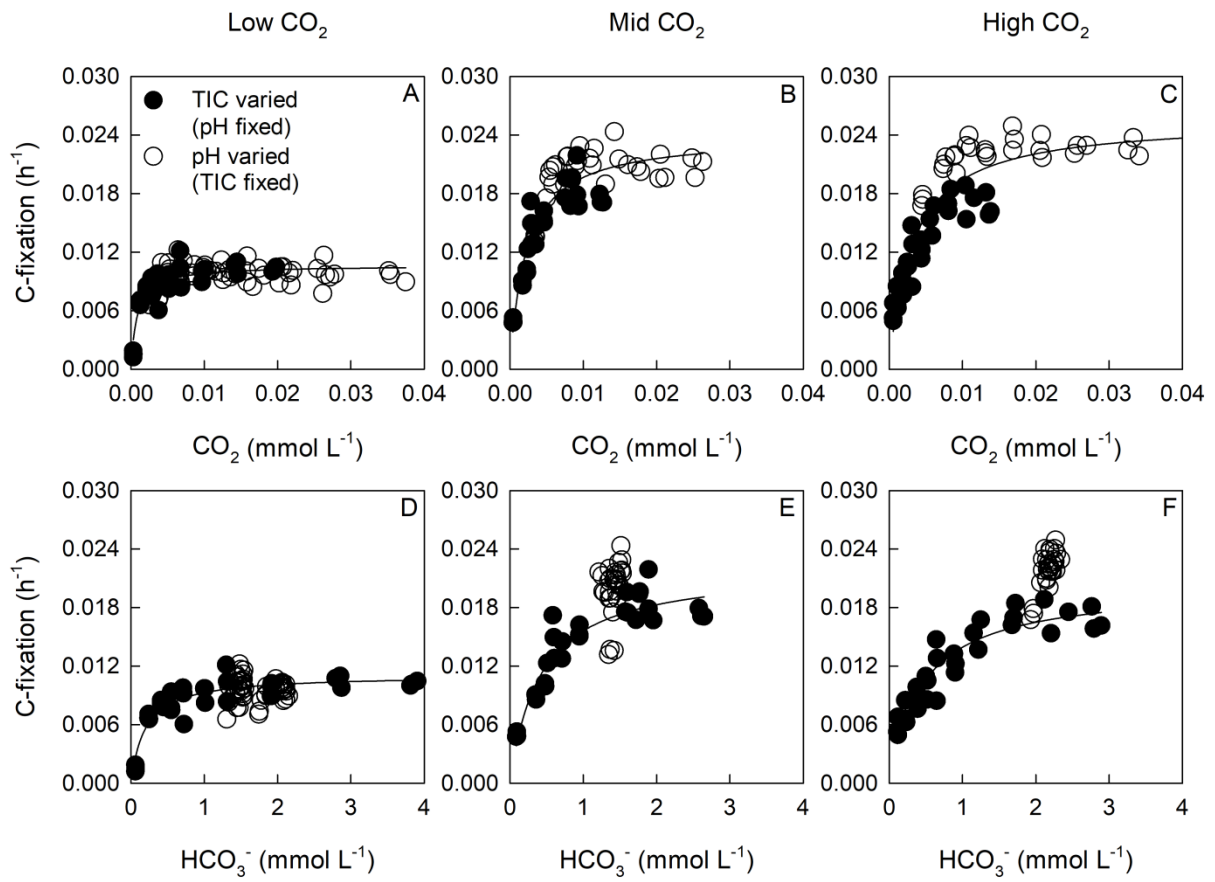
Abbreviations; V_m^C , the C-specific maximum C-fixation rates; K_m , the half saturation constant; Affinity^C, the C-specific initial slope of the V_m^C vs CO_2 response curve.

Accepted Manuscript

Fig. 1. The CO_2 and HCO_3^- response curves for inorganic C-fixation by *T. erythraeum* IMS101. C-fixation rates are normalised to a carbon (h^{-1}) basis. Data indicated by filled circles were obtained by varying TIC and HCO_3^- (mmol L^{-1}) at a fixed pH of ~ 8.15 (A-C). Data indicated by unfilled circles were obtained by varying pH ($\sim 7.52 - 8.54$) at a fixed TIC (D-F). Differences in the range of HCO_3^- and CO_2 gradients between CO_2 treatments are due to variability in pipetting and not from instability in the C_i chemistry. For the CO_2 response, curve fitting was performed using all replicates from both the TIC and pH gradients. For the HCO_3^- response, curve fitting was performed using data from the TIC gradient only. The CO_2 and HCO_3^- response curves for individual experiments are shown in Fig. S6-S11.

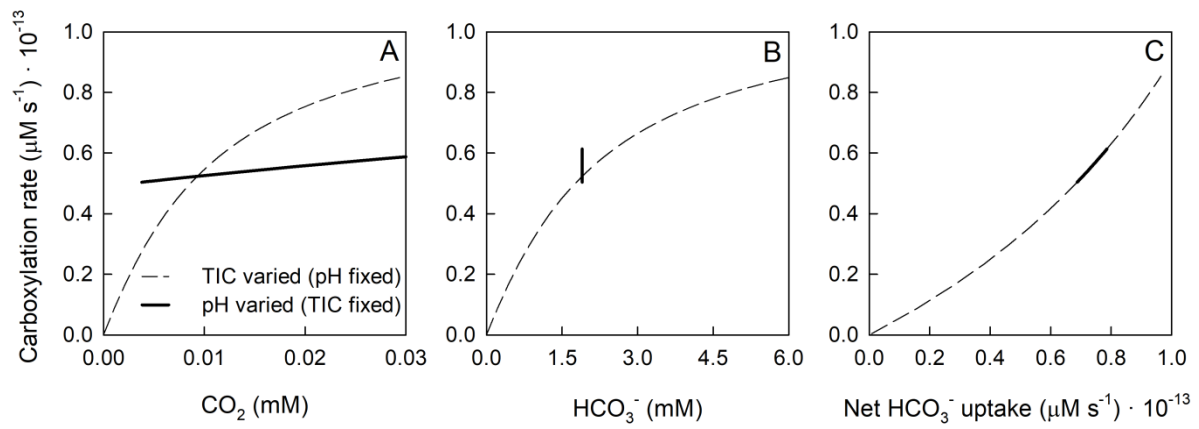
Fig. 2. The numerically calculated carboxylation rates ($\mu\text{M s}^{-1}$) obtained from the model simulations for *T. erythraeum* IMS101 as a function of external CO_2 (A) and HCO_3^- (B) concentrations; where TIC (i.e. HCO_3^-) was varied at a fixed pH = 8.15 (dashed lines) and pH was varied at a fixed $\text{HCO}_3^- = 1.9$ mM (solid lines). Carboxylation rates are also plotted against the net HCO_3^- uptake rate (C), where HCO_3^- and CO_2 leakage rates were subtracted from the rate of gross HCO_3^- transport.

Figure 1



Accepted

Figure 2



Accepted Manuscript